Available online at www.sciencedirect.com
SCIENCE DIRECT
Polymer 47 (2006) 5071–5079
polymer
www.elsevier.com/locate/polymer

High temperature behaviour of the crystalline phases in unfilled and clay-filled nylon 6 fibers

C. Ibanes [a], M. de Boissieu [b], L. David [a,1], R. Seguela [a,*]

[a] Groupe d'Etudes de Métallurgie Physique et de Physique des Matériaux, INSA de Lyon, 69621 Villeurbanne, France
[b] Laboratoire de Thermodynamique et de Physico-Chimie Métallurgique, INPG, 38402 St Martin d'Hères, France

Received 8 February 2006; received in revised form 25 April 2006; accepted 11 May 2006
Available online 26 May 2006

Abstract

Temperature-induced crystalline phase transitions in neat nylon 6 fibers as well as nylon 6/montmorillonite nanocomposite fibers have been studied by means of wide-angle X-ray scattering. Both types of melt spun fibers only consist of the γ crystalline phase that does not display any transition during heating up to the melt. In contrast, fibers drawn up to the maximum draw ratio at 140 °C display the single α phase with a high degree of chain orientation. During the temperature increase, the α phase undergoes a gradual structural disordering but preserves its monoclinic character up to melting. The structural evolution of the α form turned out sensitive to the thermal and mechanical treatment of the fibers. Annealing the unfilled drawn fibers at 150 °C prior to the WAXS experiment improves the thermal stability of the α form due to healing of the processing-induced crystalline defects. The montmorillonite-filled fibers display both the α and the γ crystals, which readily turn into α crystal form only upon drawing. Due to the matrix shearing between the MMT platelets, the H-bonded sheets display a higher thermal stability as compared with unfilled drawn fibers. Upon cooling from the melt, the first signs of crystallization are of γ form in the MMT–PA6 fibers, but the α form rapidly turns predominant. Crystallization kinetics considerations are put forward to account for this finding.
© 2006 Elsevier Ltd. All rights reserved.

Keywords: Nylon 6; Fiber; Nanocomposite

1. Introduction

Nylon 6, otherwise polyamide 6, crystallizes with two crystalline forms. The more stable α form is monoclinic [1], with H-bonded sheets between anti-parallel planar chains, (with two main characteristic reflections from the (200) and (002/202) planes) whereas the metastable γ form is pseudo-hexagonal [2] with H-bonded sheets between parallel twisted chains, with a strong dissymmetric reflection consisting of (001) and (200) close components, together with a (020) reflection. These indexations assume that the chain direction is parallel to the *b* unit cell axis. For both structures, the hydrogen (H) bonds between the amide groups lie within well-defined crystallographic planes that build up a sheet-like structure.) In the α form, the H-bonds build up a sheet-like structure between anti-parallel planar chains, (within (002) planes). In the γ form, the H-bonded sheet-like structure sets up between parallel twisted chains, (within (200) planes). The α form generally grows by slow cooling from the melt, or develops upon annealing or drawing. The γ form is obtained by fast cooling from the melt, notably in the case of fibers spun at moderate spinning rates [3,4]. Reversible chemical treatment of nylon 6 films via polyiodide complexation is also well-known to generate a very high content of γ form (after regeneration of the nylon 6 matrix by thiosulfate treatment) [5,6]. More recently, nanofillers such as natural or synthetic clays have been reported to behave as γ nucleating agents [7–11].

Most nylons have been shown to exhibit a high temperature phase transition between the stable monoclinic α form and a hexagonal form, as judged from wide-angle X-ray scattering (WAXS) or electron diffraction. The so-called Brill transition manifests itself by a gradual shift of the two main WAXS reflections of the α form, which merge into a single one characteristic of a hexagonal structure [12]. Some nylons display a clear cut Brill transition far below the melting point (Tf) while some ones retain the α crystal structure up to the

* Corresponding author. Address: Laboratoire Structure et Propriétés de l'Etat Solide, Université de Lille 1, 59655 Villeneuve d'Ascq, France. Tel.: +33 3 20 43 49 13; fax: +33 3 20 43 65 91.
E-mail addresses: laurent.david@univ-lyon1.fr (L. David), roland.seguela@univ-lille1.fr (R. Seguela).
[1] Present address: Laboratoire des Matériaux Polymères et des Biomatériaux, ISTIL, Université de Lyon 1, 69622 Villeurbanne, France.

0032-3861/$ - see front matter © 2006 Elsevier Ltd. All rights reserved.
doi:10.1016/j.polymer.2006.05.025

melting point [13–17]. Nylon 66 and nylon 6, which are closely related from both chemical and physical standpoints, are rather different regarding the Brill transition. Literature data strongly suggests that nylon 66 belongs to the first group, while nylon 6 is more probably related to the second group [18–23].

In all cases, the Brill transition is very gradual, as judged from the very large temperature domain over which the two main α reflections merge into a single one. Several studies regarding nylon 66 dealt with the question of the thermodynamic nature of the transition. Based on thermal behaviour and X-ray scattering, Starkweather and Jones [24] as well as Ramesh et al. [19] concluded to a 1st order transition, whereas Xenopoulos and Wunderlich [25] advocated in favour of a crystal packing transition. The later hypothesis is notably supported by the high thermal-history dependency of the transition [25]. The co-existence of two phases that is a necessary condition for a thermodynamic transition at phase equilibrium has been reported only by Ramesh and Gowd [23] in the case of nylon 6. This finding was unfortunately not debated by the authors. Besides, it does not mean that phase equilibrium was actually achieved.

Kinetic aspects of the phase transformation have never been taken into account, although all experimental approaches required finite recording time. In any case, thermal equilibrium does not mean thermodynamic equilibrium. Therefore, comparisons between various investigations may only be worth on a qualitative standpoint.

For nylons, which display a clear cut Brill transition far below Tf, the high temperature (HT) hexagonal structure is very close to the γ structure from the standpoint of WAXS: the two structures are characterized by a strong reflection at about the same angular position. However, from a purely crystallographic standpoint no confusion can be made between the two structures: the H-bonded sheets consist of parallel chains in the γ from, while the HT hexagonal form retains the H-bonded sheets with anti-parallel chains of the α form. This assertion is based on the following findings. On the one hand, Atkins and co-workers have claimed that the Brill transition of a great variety of nylons is associated with the librations of the methylene sequences, with a possible concomitant flip–flop of the amides groups out of the H-bond planes [14,15]. In this hypothesis, the amide flip–flop activation would be the determining factor for the Brill transition occurrence in relation to the specific chain structure and the crystalline perfection of every nylon sample. However, after being heated above the Brill transition temperature, the α form always recovers itself upon cooling. This means that the dynamic amide flip–flop does not permanently alter the typical α form H-bonding between anti-parallel chains. On the other hand, considering the γ form of nylon 6, the heating up to temperature range between the supposed Brill transition and the melting point does involve major modifications in the γ crystal structure, which is thoroughly preserved after subsequent cooling to room temperature [23,26]. These are two pieces of evidence that the H-bonded sheets are not significantly affected up to Tf, for any of the two crystal forms of nylons.

Nylon 6 deserves a particular attention in consideration of some conflicting findings in literature. The Brill transition is strongly sensitive to crystallization conditions: it may appear either far below Tf in the case of melt-crystallized samples [18], or very close to it or not at all in the case of single crystals grown from solution [17]. It is worth noticing the assumption by several authors that the angular separation between the two main reflections of the nylon 6 α structure, as measured at room temperature, depends on the degree of crystal perfection or crystal size [27–30], in relation to processing. So, one may wonder if the variation of this angular separation with temperature for a given sample has the similar origin, i.e. an increasing concentration of crystal defects. It is also worth noticing that the Brill transition is dependent on chain length as judged from the peculiar behaviour of nylon 6 oligomers as compared with polymers [17].

In recent years, nanocomposites based on nylon 6 matrix and clay nanofillers have aroused great interest due to a spectacular thermo-mechanical reinforcement at temperature above the glass transition, for rather low clay contents [31,32]. The clay platelets have a noticeable γ-nucleating effect [7–11] that is suspected to contribute to the reinforcement through the build up of a rigid percolating network of crystalline lamellae and clay platelets [10], in addition to the very high aspect ration of the clay particles.

Fibers spun from such kind nanocomposites were recently investigated from the standpoint of structure–mechanical property relationships [11]. Improved stiffness and strength were observed for the drawn clay/filled fibers as a result of an enhanced drawability. Temperature effects on properties and structure were not studied yet. The present study deals with the temperature dependency of the crystalline structure of such spun and spun-drawn fibers.

2. Experimental

The polyamide 6 (PA6) matrix had a weight-average molar weight $M_w \approx 80$ kDa and a polydispersity index $I \approx 2$. Yarns, about 30 μm in diameter, were melt spun at 260 °C, using a winding speed of 800 m/min. Bundles of 10 single yarns were winded up together to form the so-called fibers that will be used in this study. The fibers were drawn at a temperature of 140 °C. The maximum draw ratio, λ_{max}, is given by the ratio of the sample length after drawing close to rupture to the length prior to drawing. PA6 filled with 1% by weight of montmorillonite (MMT) was also used for spinning fibers. The MMT particles were surface-treated with about 40% by weight of dimethyl-dioctadecyl-quaternary-ammonium surfactant for exfoliation during compounding with PA6. In the previous study [11], transmission electron microscopy revealed a rather fine MMT platelet dispersion in the spun fibers, with a clear-cut orientation parallel to the fiber axis. This observation was supported by small-angle X-ray scattering that revealed almost isolated platelets from the curve fitting of the strong equatorial scattering profile, as well as by the absence of characteristic wide-angle X-ray scattering of MMT tactoids [11].

The wide-angle X-ray scattering (WAXS) study was carried out in transmission mode using a point-focusing collimation. The Cu– Kα radiation was selected with a graphite monochromator from a Rigaku rotating anode operated at 40 kV and 100 mA and having a focus size of 0.3 mm. The scattering intensity was collected on a two-dimensional CCD camera from Roper Scientific. The patterns were corrected for background scattering and for the geometry and intensity distortions of the CCD camera. The samples consisted of 40 fibers held parallel to each other in a sample holder. The latter was inserted into a small oven equipped with thin Kapton windows. The samples were heated at a rate of 1 °C/min. Every recorded pattern was an average of six acquisitions of 30 s, so that the actual sample temperature evolved over a 3 °C domain during the recording. This drawback of the heating procedure allows limiting thermal degradation due to long isothermal experiments in the temperature range of the melting point.

In order to separate the various contributions to the WAXS patterns of the oriented fibers, and to determine the weight-fractions of the α and γ crystalline phases and the overall crystallinity, the patterns were integrated over a 90° azimuthal sector from equator to meridian divided into 10° azimuthal sectors and analyzed. Pearson VII functions were used to fit the various contributions to the intensity profile following a previously described procedure [11]. Fig. 1 shows an example of decomposition involving an amorphous scattering, two α reflections and three γ reflections in the scattering angle domain $7° < 2\theta < 29°$. For the sake of simplicity, α_1 and α_2 hold for the (200) and (002/202) reflections of the α form, whereas γ_1, γ_2 and γ_3 hold for the (001), (200) and (020) reflections of the γ form, respectively. In addition, the discussions dealing with the α_2 reflection will be made with regard to the sole (002) contribution, considering that the (202) contribution is minor in first approximation [33].

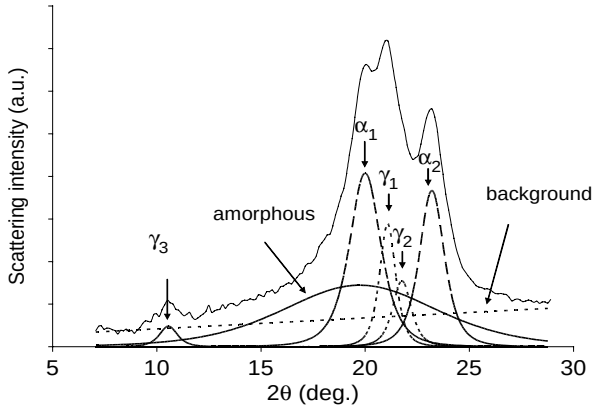

Fig. 1. Principle of the WAXS intensity profile decomposition in the case of the equatorial scattering sector recorded at room temperature from a MMT–PA6 spun fiber (the α_1 and α_2 peaks hold for the (200) and (002/202) reflections of the α form, respectively; the γ_1, γ_2 and γ_3 peaks hold for the (001), (200) and (020) reflections of the γ form, respectively).

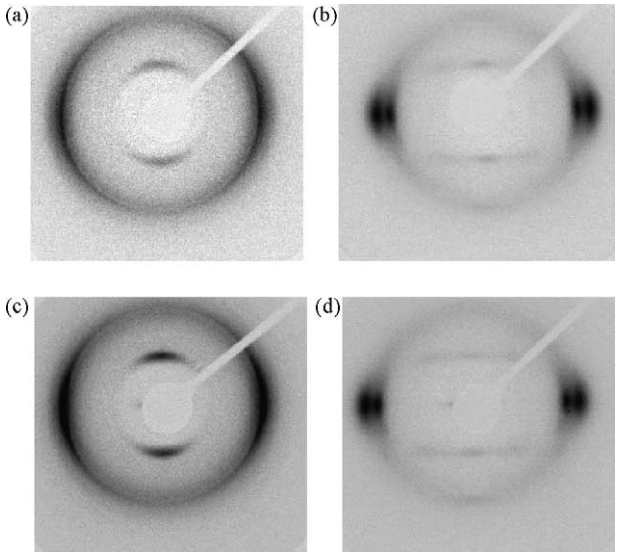

Fig. 2. WAXS patterns at room temperature of a PA6 fiber (a) as-spun and (b) drawn at $\lambda_{max} = 2.65$, and of a MMT–PA6 fiber (c) as-spun and (d) drawn at $\lambda_{max} = 3.05$ (the fiber axis is vertical).

3. Results and discussion

The WAXS diagrams from PA6 and MMT–PA6 spun fibers at room temperature are reported in Fig. 2. Both kinds of spun fibers display a typical γ form structure. Both fibers also display a marked crystalline orientation parallel to the fibers axis. It is worth noting a very faint equatorial scattering close to the beam stop in the case of the MMT–PA6 fiber that is relevant to the presence of the MMT platelets having a marked orientation parallel to the fiber axis, i.e. the spinning direction [11]. The two kinds of fibers drawn up to λ_{max} display a much stronger crystalline orientation than their spun parents. The occurrence of the main α_1 and α_2 reflections of the α form is relevant to the well-known strain-induced γ–α phase transition. The decomposition procedure of the intensity profiles does not reveal any remnants of γ crystals for the two fibers drawn at λ_{max}. Table 1 reports the crystal weight fraction data for the various fibers as determined from the WAXS analysis. Besides, the increase in chain orientation, plastic drawing imparts a significant increase in crystallinity that can be ascribed to the chain-unfolding. Indeed, considering that the linear PA6 chains with no stereo-regularity problems have very high crystallization potential, drawing offers an opportunity to the amorphous chain folds that undergo unfolding to crystallize via strain-induced chain alignment.

Table 1
Weight fraction crystallinity, W_c, of the fibers at room temperature

Fibers	W_c (±2%)
PA6 as-spun	35
PA6 $\lambda_{max} = 2.65$	52
MMT–PA6 as-spun	42
MMT–PA6 $\lambda_{max} = 3.05$	61

3.1. Temperature evolution of the γ crystalline phase and amorphous phase

The equatorial WAXS intensity profiles of the as-spun MMT–PA6 fiber are reported in Fig. 3 as a function of temperature. The typical γ phase scattering profile with the predominant γ_1 reflection at $2\theta \approx 21°$ is preserved up to melting, indicating that the γ phase is thermodynamically stable. This is consistent with previous data from isotropic γPA6 films produced by iodine treatment [23,26]. Only a slight shift to lower scattering angle of this reflection can be observed as a result of thermal dilatation of the γ unit cell in its basal plane. It is worth noticing that, in contrast to the above findings, examples have been reported of unstable γ crystals, which transform into α form before the thermodynamic melting point [3,10,34]. It is not known if the phase transition is a melting-recrystallization process of highly defective crystals or a gradual solid-state reorganization.

3.2. Temperature evolution of the α crystalline phase

Fig. 4 displays the WAXS profiles as a function of temperature of the neat PA6-fiber drawn at $\lambda_{max} = 2.65$. In contrast to the evolution of the γ form, the present α form WAXS profiles are strongly dependant on temperature. The main α_1 and α_2 reflections shift close to each other with increasing temperature and seem to merge into a single reflection above 190 °C. Previous studies reported the occurrence of two or even three new reflections in the course

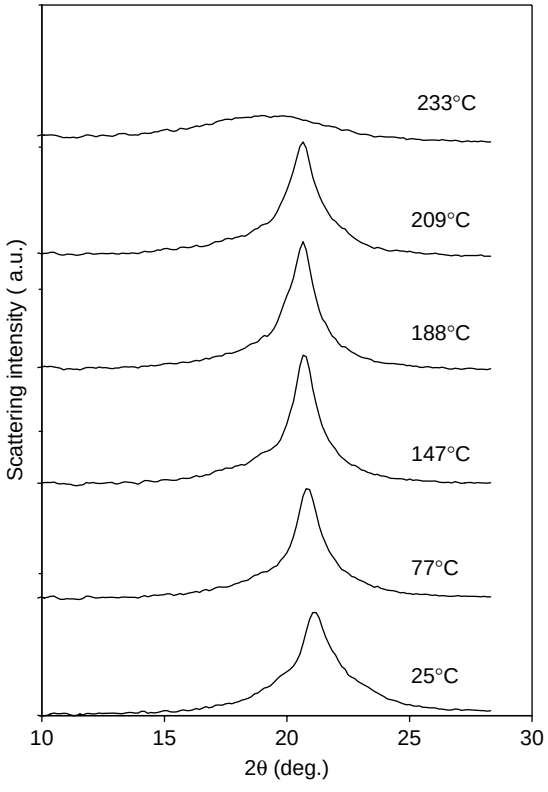

Fig. 3. Equatorial WAXS intensity profiles as a function of temperature for the as-spun MMT–PA6 fiber.

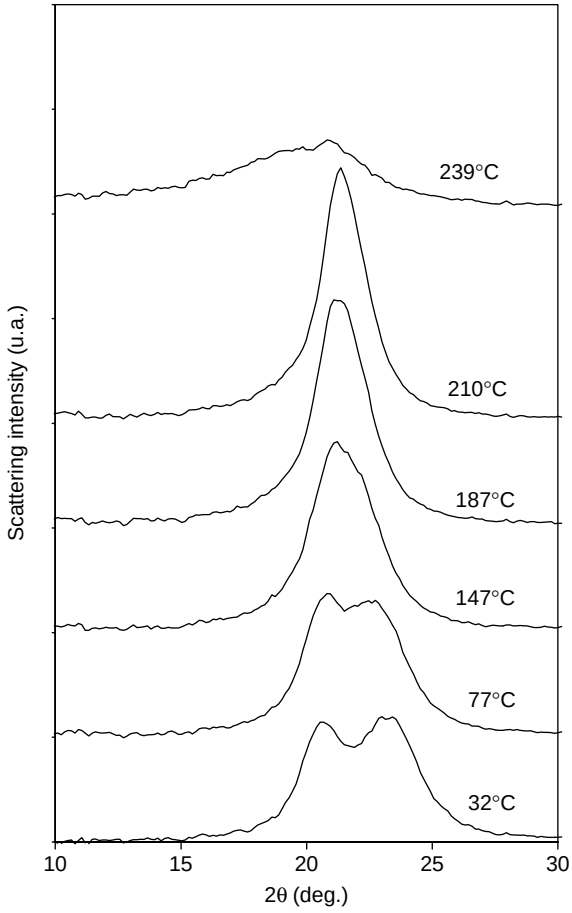

Fig. 4. Evolution with increasing temperature of the WAXS equatorial profiles of the neat PA6 fiber drawn at $\lambda_{max} = 2.65$.

of the heating [18,23], which were ascribed to a new crystalline form and the Brill transition, before the disappearance of the main α_1 and α_2 reflections. The present WAXS results could not be treated in the assumption of such new phase occurrence. The two Bragg spacings of the α_1 and α_2 reflections have been computed and plotted in Fig. 5 as a function of temperature. The temperature dependence of the two reflection spacings is similar to that reported for most nylons in α form, including nylon 6. This phenomenon is not simply due to thermal dilatation considering that the α_1 spacing decreases with increasing temperature. As suggested by Atkins and co-workers [14–17], this is more likely due to H-bond redistribution between and within the H-bonded sheets, because of thermal activation of amide group flip–flop. The two reflections never merge into a single one, which means that the Brill transition does not occur before melting. According to Atkins et al. interpretation, the α crystal form of the PA6 drawn fiber is rather resistant to H-bonding randomization.

It is noteworthy that above 220 °C, the α_1 and α_2 reflections are shifting away from each other suggesting the occurrence of new structure, as already claimed by Ramesh and Gowd [23]. In addition, it is quite surprising that the two reflections still exist at 240 °C, i.e. above the thermodynamic melting point. This finding gives evidence of the persistence above

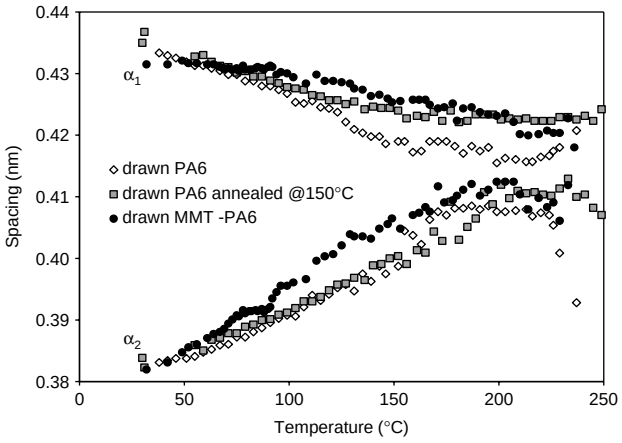

Fig. 5. Evolution with increasing temperature of the α_1 and α_2 spacings for (◇) the PA6 drawn fibers, (□) the annealed PA6 drawn fibers and (●) the drawn MMT–PA6 fibers.

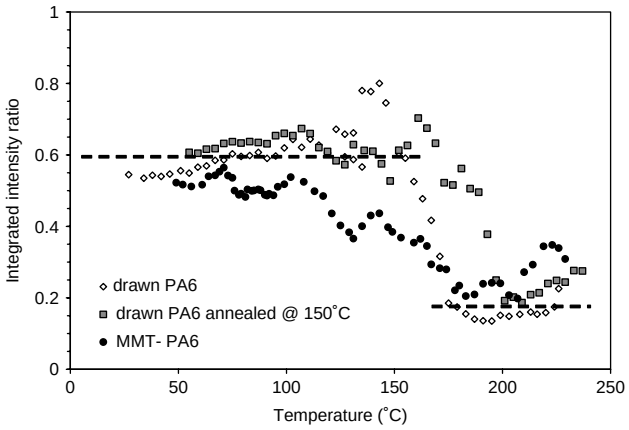

Fig. 6. Evolution with increasing temperature of the α_1/α_2 integrated intensity ratio for (◇) the PA6 drawn fibers, (□) the annealed PA6 drawn fibers and (●) the drawn MMT–PA6 fibers.

the melting point of stable crystalline nuclei, a well-known phenomenon in semi-crystalline polymers, more peculiarly nylons [35].

For the sake of comparison, PA6 fibers drawn up to λ_{max} and subsequently annealed for 30 min at 150 °C with fixed ends have been studied in parallel, together with MMT–PA6 fibers drawn to $\lambda_{max}=3.05$. The temperature dependency of the α_1 and α_2 spacings reported in Fig. 5 is less for the annealed PA6 drawn fiber than for the parent fiber prior to annealing, notably in the 180–240 °C range where no significant trend of shifting away from each other of the two reflections is observed. The annealed α form is more stable after the annealing treatment.

An explanation for this effect is that annealing improves the crystalline perfection by reducing the processing-induced crystalline defects. In the framework of Atkins et al. mechanism for the Brill transition, on may assume that the H-bond distribution within (002) sheets of the perfect α unit cell may not be obeyed in spun and spun-drawn fibers due to processing conditions, which do not enable perfect rearrangement of all the H-bonds during the crystallization step. As suggested by Murthy et al. [36], some H-bonds may randomly be formed between (002) planes instead of within these planes, accompanied with a conformational defect of the amide group in the chain: the higher the concentration of such crystallographic misfits, the larger the departure of the α_1 and α_2 spacings from the values of the ideal α structure. This interpretation borrows from Ziabicky model for the nylon 6 mesomorphic β form [37], which assumes a hexagonal symmetry accompanied with a random distribution of H-bonds about the chain axis. During the annealing treatment, the frozen in defects promote the mobility activation of the chains and enable them to adopt the most stable conformation during the subsequent cooling, giving thus the opportunity to a maximum number of H-bonds to settle within the (002) sheets.

It is worth noticing that the improved thermal stability after annealing of the PA6 drawn fibers may be the reason for the efficiency of the so-called heat-setting that is commonly achieved at an industrial level to enhance dimensional stability after spinning and drawing of nylon 6 fibers [38–40].

The fact that the spacing differences between the various fibers do not exceed about 0.05 Å (Fig. 5), i.e. the order of magnitude of the measurement accuracy, makes irrelevant further discussion on these spacing variations. However, better insight into the temperature-induced crystal changes of the fibers can be afforded through the α_1/α_2 integrated intensity ratio that has been plotted in Fig. 6 as a function of temperature, for the three drawn fibers. Such kind of measurements has been already reported in literature [18,23], but the physical meaning of its evolution was not discussed. This ratio is close to 0.6 at low temperature, in agreement with intensity data from Holmes et al. [1] for isotropic films. Then it drops to about 0.2 at high temperature for the three fibers. Considering that the intensity of a given reflection is proportional to the amount of scattering matter in the corresponding plane, the above finding means that the (200) planes of the α form are more disturbed by the temperature increase than the (002) planes. The latter planes are the ones that form the sheet-like structure, so that one may expect a greater internal cohesion of the H-bonded sheets that preserves their periodic stacking. In contrast, the weakening with increasing temperature of the van der Waals inter-sheet interactions mainly due to the methylene moieties librations is likely to allow misfits in the H-bonded sheet stacking so that the (200) planes will undergo increasing crystallographic disorder. Notwithstanding, the sheet-like structure for the three kinds of fibers does collapse before the melting temperature is reached.

Regarding the specific behaviour of every fiber, the annealed PA6 drawn fiber seems to be more resistant to temperature than the other two ones as judged from the preservation of the ratio $\alpha_1/\alpha_2=0.6$ up to 180 °C. This is consistent with the improved thermal stability previously concluded from the evolution of the α_1 and α_2 spacings. In contrast, the MMT–PA6 drawn fibers look more sensitive to temperature as can be seen from the early drop of the α_1/α_2 ratio. This suggests lesser thermal stability of the (200) planes as compared with the (002) planes, in other words better crystallographic order for the former planes. As a tentative explanation, one should consider on the one hand the

solid-state γ–α strain-induced transition of the MMT–PA6 fibers upon drawing and, on the other hand, the higher shear compliance of the (200) H-bonded sheets of the α form, which provides them with a greater ability to orient parallel to the shear stress. One may thus suggest that the shearing of the PA6 matrix confined between the rigid MMT platelets compels the α form H-bonded sheets to orient themselves parallel to MMT surface. This phenomenon compares with the shear amplification mechanism reported to occur during the injection-moulding of MMT–thermoplastic nanocomposites [41–43]. The structural reordering during the strain-induced phase transition is thus likely to be more active in the (002) planes than in the (200) owing to the help of the MMT platelets. Indeed, in addition to the parallel stacking of the (002) H-bonded planes, the construction of the (200) planes of the α form during the plastic drawing requires a very high degree of lateral ordering of the former ones, which is only partly achieved due to internal stresses and the weak van der Waals interactions between the sheets. A correlation could be made between this kind of stacking disorder and the well-known inter-sheet shear described by Atkins and co-workers [14–16] for various kinds of nylons and more particularly for nylon 6 oligomers [17]. In the present instance of drawn MMT–PA6 fibers, the occurrence of conformational defects involving H-bonds out of the H-bonded sheets may be expected to reduce the regularity of the inter-sheet shear.

It is worth noticing that the mutual orientation of the rigid MMT platelets and the strong internal cohesiveness of the H-bonded sheets parallel to the fiber axis is a cooperative process that drives the material through the minimum energy pathway during the plastic drawing. This kind of structural organization precludes the build up of H-bonds between the PA6 chains and the MMT platelets, only van der Waals interactions can be established between matrix and filler. As a direct consequence, MMT–PA6 fibers and neat PA6 fibers exhibit equivalent stiffness at similar draw ratio [11]. This effect contrasts with the well-known mechanical reinforcement of bulk nylon 6/clay nanocomposites that was ascribed to the epitaxy-like growth of γ crystals onto the clay platelets [44,45] and the concomitant clay platelets bridging by the crystalline lamellae [9,46,47]. In the present case of drawn PA6 fibers, the major benefit from the MMT platelets is an improved drawability resulting in a higher stiffness of the MMT–PA6 fibers as compared with the unfilled PA6 fibers [11].

3.3. Structural change during cooling

After heating the fibers up to 240 °C, WAXS investigations has been continued during the cooling step, at a cooling rate of about 2–3 °/min. The molten fibers stayed in place in the sample holder owing to the sticking of the molten material to the Kapton windows of the heating cell. Fig. 7 shows the WAXS patterns of the PA6 and MMT–PA6 fibers at 60 °C, during the cooling step. For both materials, the nearly uniform pattern indicates that the chains have relaxed and recovered a random coil conformation when the sample was heated up to the melting point, before recrystallization of the material in an

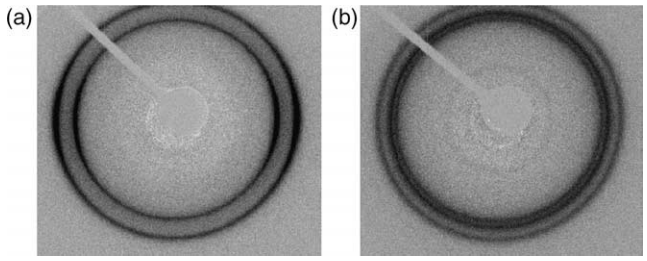

Fig. 7. WAXS patterns of (a) PA6 fiber and (b) MMT–PA6 fiber at 60 °C, during the cooling step after heating up to the melt.

isotropic state during the subsequent cooling. For the PA6 fiber, the narrowness of the α_1 and α_2 reflections of Fig. 7(a) contrasts with the broadness of the corresponding reflections of the drawn PA6 fiber (Fig. 2(b)). This emphasizes the role of plastic drawing in the crystal defectiveness as compared to crystallization from the quiescent melt that obviously enables the growth of almost defect-free crystals.

Fig. 8 shows the detailed evolution of the α_1 and α_2 spacings of the PA6 fiber during the course of the slow cooling. In contrast to the observations during heating (Fig. 5), very little evolution of the spacings occurs, indicating that a high degree of crystalline perfection develops as soon as the first crystals appear, and during further growth of crystals upon cooling. The activation of methylene librations can be a driving force to the development of α crystals having high degree of crystallographic perfection. On the one hand, local chain mobility is required for the chains to reach the lower potential energy conformation insuring an optimum thermal stability, with notably all H-bonds formed in adequate position. On the other hand, only perfect crystals with optimum interactions can resist the thermal disordering responsible for the Brill transition. This interpretation for the α_1 and α_2 spacing evolution suggests that the temperature and the processing sensitivities of the α phase have an analogous origin, namely crystallographic defects in relation to the more or less perfect distribution of the H-bonds within well-defined planes.

In the case of the MMT–PA6 fiber, after slow cooling from the melt down to at 60 °C (Fig. 7(b)), the γ_1 reflection clearly appears in the interval between the α_1 and α_2 reflections, together with a faint γ_3 reflection. This finding corroborates

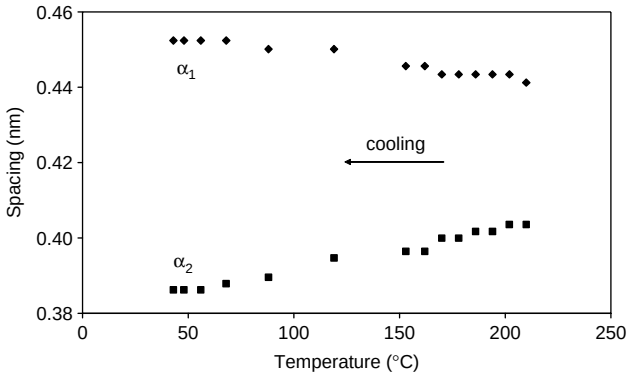

Fig. 8. Evolution with decreasing temperature of the α_1 and α_2 spacings for the PA6 spun fibers after heating up top the melt.

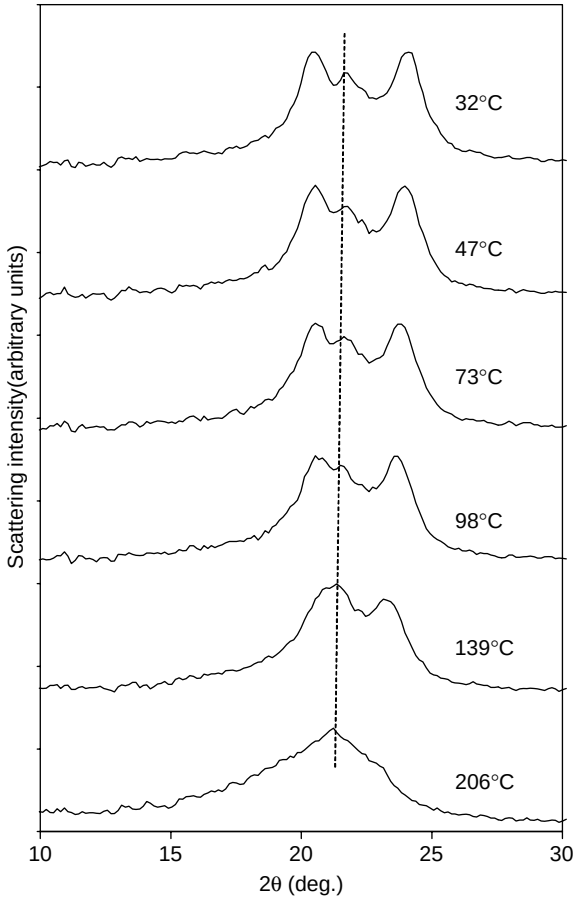

Fig. 9. Evolution with decreasing temperature of the WAXS equatorial profiles of the MMT–PA6 fibers.

the already claimed γ-nucleating effect of the MMT platelets on PA6. Equatorial WAXS profiles for the MMT–PA6 fiber are shown in Fig. 9 as a function of temperature, during the slow cooling from the melt. The γ_3 reflection seems to occur first at 206 °C. Then the α_1 and α_2 reflections gradually develop with decreasing temperature, whereas the γ_3 reflection intensity seemingly remains constant. Although this observation confirms the γ-nucleating effect of the MMT platelets, the α structure is obviously the preferred crystalline form in the case of slow cooling of MMT–PA6 from quiescent melt, as compared with melt spinning.

The predominance of α phase upon slow cooling of the MMT–PA6 fiber from the quiescent melt may have two origins. The α crystals may grow sporadically in the PA6 matrix without connection to the initially grown γ crystals, and invade the whole PA6 matrix faster than the γ phase due to kinetic predominance of α form at high temperature [50]. Alternatively, the earlier γ crystals nucleated on the MMT platelet surface may work as precursory nuclei for the α phase as the growth front of the crystals moves off the platelet surface, due to thermodynamic stability of the later crystal form. In that instance, a kind of epitaxy can be expected at the border between the two crystal forms. As a matter of fact, the γ–α phase change during the crystal growth in PA6 does not require tremendous structural rearrangements, since a cooperative twist of the chain about the amid groups only enables the H-bonded parallel chains of the γ form to switch to the H-bonded anti-parallel chains of the α form [48,49]. The fact that the γ form appears as the minor crystalline component at the end of the cooling, in spite of its early appearance during the course of the cooling (Fig. 9), is a voucher in favour of the second proposal. The present WAXS data are, however, not definitively conclusive on that question. DSC data from the previous study [11] bring about additional support to the second proposal: the molten MMT–PA6 fiber displays a single crystallization exotherm at a cooling rate of 10 °C/min, the onset and the peak temperatures of which are roughly identical to those of the molten PA6 fiber. This suggests that both MMT–PA6 and neat PA6 obey the same overall crystallization kinetics, namely that of the α form, in spite of the initial γ-nucleating effect of the MMT platelets. This is afforded via the higher growth rate of the α crystal form as compared with the γ form at high temperature, or under slow cooling conditions [50]. Besides, the single exotherm does not support the sporadic growth of α crystals independently from the γ phase growth: indeed, two exothermic peaks or at least a significant peak broadening should be rather expected. A last point in favour of the second proposal is the analogy of the present situation with the case of isotactic polypropylene [51] for which, in spite of a very weak nucleation rate, β crystals develop faster than α crystals thanks to 'growth transformation' onto the surface of the α spherulites. The analogy between PP and PA6 relies on both the different growth rates of the two crystal forms and the occurrence of a switch of crystal form growth during the course of crystallization.

Although the decomposition procedure into individual contributions enables detecting the two main reflections of the α form at its earlier stage of growth from the melt, as revealed from the data of Fig. 8 regarding neat PA6 fibers, additional information about the building of the crystalline structure upon cooling appear in the WAXS patterns of Fig. 9 concerning MMT–PA6 fibers. At 139 °C, the clear cut appearance of the α_2 reflection contrasts with the very slight hump associated with the α_1 signal. This latter reflection only appears as a faint peak at 98 °C, and then becomes a well-formed α_1 reflection at about 47 °C. In consideration of the previous discussion about the α_1 and α_2 spacing evolution in neat PA6 fibers upon cooling (Fig. 8), this quite different intensity evolution of the two α reflections strongly suggests that most of the (002) H-bonded sheets are formed at a very early stage of crystallization. In contrast, only very limited domains in the molten material contain well-organized (200) planes at high temperature, leading to a very faint signal that can be only revealed via spectral decomposition. Decreasing temperature strengthen the inter-sheet van der Waals interactions promoting thus better crystallographic stacking of the H-bonded sheets. This results in α_1 reflection increase due to gradual growth of domains with well-built (200) planes. This interpretation is consistent with the proposal by Wunderlich et al. [52] that a mesomorphic state exists between the liquid and the crystal, along the crystallization pathway. The above result also supports the previous conclusion that

the (200) planes have lesser thermal stability than the (002) planes, irrespective of the fiber composition and processing conditions, as judged from the α_1/α_2 ratio evolution with increasing temperature.

4. Concluding discussion

The thermal stability of the α crystal structure in drawn PA6 fibers is confirmed to be sensitive to processing and thermo-mechanical treatment Annealing of drawn PA6 and MMT–PA6 fibers involves a reduced temperature sensitivity of the α crystal structure. This improved thermal stability of α crystals upon annealing is ascribed to a reduction of the process-induced crystallographic defects. In the case of the MMT-filled fibers, the shearing of the PA6 matrix confined between the MMT platelets during the plastic drawing is suggested to impart better stacking and cohesion to the H-bonded (002) planes as compared with the (200) planes. The significant departure of the respective temperature of occurrence of these two planes during cooling corroborates the better thermal stability of the latter ones that form the H-bonded sheets.

The γ-nucleating role of the MMT platelets in nylon 6, often reported in literature in the case of injection-moulded samples, has been confirmed in the oriented spun fibers. However, the γ crystal growth is strongly reduced in the slow cooled fibers after heating up to melting. This finding cast doubts on the actual γ-nucleating role of the MMT platelets. It could be that the MMT platelets only have a reinforcing effect on the natural trend of nylon 6 to growth into γ crystalline form under shear and/or fast cooling conditions due to the shear amplification effect of the high aspect ratio platelets during processing. Some findings from literature regarding injection-moulded samples support this hypothesis. For instance, the decreasing shear rate across the sample thickness, from the mould surface to the sample core, has always been reported to involve a concomitant decrease of the MMT platelet orientation and the γ phase content [10,42,43,53]. The γ content in the core of such injection-moulded samples is even roughly identical to that of injected pure nylon 6, in spite of the presence of unoriented MMT platelets [53].

Recent data from Nair and Ramesh [54] revealed the predominance of γ form crystals in the case of intercalated nylon 6-cloisite nanocomposites isothermally crystallized at 100 °C. Although no shear was applied in these experiments, the predominance of γ crystals is perfectly consistent with the faster crystallization kinetics of that crystal form at low temperature [50].

The very similar dependence on crystallization temperature of the γ form content in MMT–nylon 6 systems and pure nylon 6 under quiescent conditions is a piece of evidence of the major influence on the process of the own structural habits of the nylon 6 matrix.

Finally, thermo-mechanical history was recently shown to have dramatic influence on the nucleating capabilities of MMT platelets in commercial MMT–nylon 6 hybrids: although the as-received pellets did display increasing γ-form content with increasing MMT weight fraction, a twin-screw micro-extrusion treatment at 50 rpm and 310 °C resulted in α crystals only, whatever the MMT content in the range 0.5–4 wt% [55]. Further work is in progress for determining what kind of texture the nylon 6 matrix develops about the MMT platelets in that case, and the consequence on mechanical properties.

Acknowledgements

The authors are indebted to the Région Rhône-Alpes for financial support to this work and for the grant of a doctoral fellowship to C. Ibanes. Financial and technical support from Rhodia is also acknowledged.

References

[1] Holmes DR, Bunn CW, Smith DJ. J Polym Sci 1955;17:159–77.
[2] Arimoto H, Ishibashi M, Hirai M, Chatani Y. J Polym Sci, Part A 1965;3:317–26.
[3] Gianchandani J, Spruiell JE, Clark ES. J Appl Polym Sci 1982;27:3527–51.
[4] Murase S, Kashima M, Kudo K, Hirami M. Macromol Chem Phys 1997;198:561–72.
[5] Miyasaka K, Makishima K. J Polym Sci, Part A-1 1967;5:3017–27.
[6] Murthy NS. Macromolecules 1987;20:309–16.
[7] Kojima Y, Usuki A, Kawasumi M, Okada A, Kurauchi T, Kamigaito O, et al. J Polym Sci, Polym Phys 1994;32:625–30.
[8] Liu L, Qi Z, Zhu X. J Appl Polym Sci 1998;71:1133–8.
[9] Lincoln DM, Vaia RA, Wang Z-G, Hsiao BS, Krishnamoorti R. Polymer 2001;42:9975–85.
[10] Varlot K, Reynaud E, Kloppfer M-H, Vigier G, Varlet J. J Polym Sci, Polym Phys 2001;39:1360–70.
[11] Ibanes C, de Boissieu M, David L, Séguéla R, Epicier T, Robert G. J Polym Sci, Polym Phys 2004;42:3876–92.
[12] Brill R. J Prakt Chem 1942;161:49–64.
[13] Itoh T. Jpn J Appl Phys 1976;15:2295–306.
[14] Jones NA, Cooper SJ, Atkins EDT, Hill MJ, Franco L. J Polym Sci, Polym Phys 1997;35:675–88.
[15] Jones NA, Atkins EDT, Hill MJ, Cooper SJ, Franco L. Polymer 1997;38:2689–99.
[16] Jones NA, Atkins EDT, Hill MJ. Macromolecules 2000;33:2642–50.
[17] Cooper SJ, Atkins EDT, Hill MJ. Macromolecules 1998;31:8947–56.
[18] Murthy NS, Curran SA, Aharoni SM, Minor H. Macromolecules 1991;24:3215–20.
[19] Ramesh C, Keller A, Eltink SJE. Polymer 1994;35:2483–7.
[20] Androsch R, Stolp M, Raddusch HJ. Acta Polym 1996;47:99–104.
[21] Vasanthan N, Murthy NS, Bray RG. Macromolecules 1998;31:8433–5.
[22] Murthy NS, Wang Z-G, Hsiao BS. Macromolecules 1999;32:5594–9.
[23] Ramesh C, Gowd EB. Macromolecules 2001;34:3308–13.
[24] Starkweather Jr HW, Jones GA. J Polym Sci, Polym Phys 1981;19:467–77.
[25] Xenopoulos A, Wunderlich B. Colloid Polym Sci 1991;264:375–91.
[26] Penel-Pierron L, Depecker C, Séguéla R, Lefebvre J-M. J Polym Sci, Polym Phys 2001;39:484–95.
[27] Park JB, Devries KL, Statton WO. J Macromol Sci, Phys 1978;B15:229–56.
[28] Murthy NS, Minor H, Latif RA. J Macromol Sci, Phys 1987;B26:427–46.
[29] Salem DR, Moore RA, Weigmann HD. J Polym Sci, Polym Phys 1987;25:567–89.
[30] Salem DR. J Polym Sci, Polym Phys 1987;25:2561–6.
[31] Kojima Y, Usuki A, Kawasumi M, Okada A, Fukushima Y, Kurauchi T, et al. J Mater Res 1993;8:1185–9.
[32] Giannelis EP. Adv Mater 1996;8:29–35.
[33] Scattering intensity calculations for the various α nylon 6 reflections after Holmes et al. [1] indicate that the (202) contribution to the (α_2 reflection is about three times weaker than the (002) contribution.

[34] Liu X, Wu Q. Polym Commun 2002;43:1933–6.
[35] Xenopoulos A, Clark ES. In: Kohan MI, editor. Nylon plastics handbook. Munich: Hanser Publishers; 1995 [chapter 5].
[36] Murthy NS. Polym Commun 1991;32:301–5.
[37] Ziabicky A. Kolloid-Z Z Polym 1959;167:132–41.
[38] Tsuruta M, Koshimo A. J Appl Polym Sci 1965;9:3–9.
[39] Bhat NV, Kelkar DS. J Macromol Sci Phys 1989;B28:375–88.
[40] Vasanthan N. Textile Res J 2004;74:545–50.
[41] Yalcin B, Valladares D, Cakmak M. Polymer 2003;44:6913–25.
[42] Yalcin B, Cakmak M. Polymer 2004;45:2691–710.
[43] Wang K, Xiao Y, Na B, Tan H, Zhang Q, Fu Q. Polymer 2005;46: 9022–32.
[44] Maiti P, Okamoto M. Macromol Mater Eng 2003;288:440–5.
[45] VanderHart DL, Asano A, Gilman JW. Macromolecules 2001;34: 3819–22.
[46] Kim GM, Lee DH, Hoffmann B, Kressler J, Stöppelmann G. Polymer 2001;42:1095–100.
[47] Masenelli-Varlot K, Reynaud E, Vigier G, Varlet J. J Polym Sci, Polym Phys 2002;40:272–83.
[48] Penel-Pierron L, Seguela R, Lefebvre J-M, Miri V, Depecker C, Lutigny M, et al. J Polym Sci, Polym Phys 2001;39:1224–36.
[49] Aharoni SM. *n*-Nylons: their synthesis, structure and properties. New York: Wiley; 1997.
[50] Kyotani M, Mitsuhashi S. J Polym Sci, Polym Phys 1972;10: 1497–508.
[51] Lovinger AJ, Chua JO, Gryte CC. J Polym Sci, Polym Phys 1977;15: 641–56.
[52] Wunderlich B, Grebowicz J. Adv Polym Sci 1984;60–61:1–59.
[53] Fornes TD, Paul DR. Polymer 2003;44:3945–61.
[54] Nair SS, Ramesh C. Macromolecules 2005;38:454–62.
[55] Peurton F., Miri V., Elkoun S., Lefebvre JM., Lacrampe MF., Krawczak P. Proceedings of the polymer nanocomposites conference. National Research Council of Canada, Montreal, CD-ROM pdf file. 4.02 2005.